Porous Crystalsomes via Emulsion Crystallization and Polymer Phase Separation

Mark C. Staub, Seyong Kim, Shichen Yu, and Christopher Y. Li*

Department of Materials Science and Engineering, Drexel University, Philadelphia, Pennsylvania, 19104 United States

ABSTRACT: Crystalsomes are crystalline capsules that are formed by controlling polymer crystallization to break translational symmetry. While recent studies showed that these crystalline capsules exhibit interesting mechanical properties, thermal behavior, and excellent performance in blood circulation, the closed capsule is undesired for drug delivery applications. We report the formation and characterization of porous crystalsomes where porosity is rendered on the crystalline shells. A miniemulsion is formed using two amphiphilic block copolymers (BCP). The competition between controlled crystallization and phase separation of the BCPs at the emulsion surface leads to multiphase crystalsomes. Subsequently removing one BCP produces porous crystalline capsules.

Porous polymer nanoparticles have attracted significant interest in the past few decades because of their high specific surface area which is essential for drug delivery, catalysis, and energy storage applications.[1-5]A variety of strategies have been used to generate porous polymer particles, including suspension polymerization,[6, 7] precipitation polymerization,[7, 8] dispersion polymerization,[9] seeded suspension polymerization,[10] membrane/microchannel emulsions,[11] and microfluidics.[12-14] Block copolymer (BCP) phase separation has also been utilized to create pores in polymersomes.[15-17] For example, Discher *et al*. reported polymersomes formed by a mixture of poly (ethylene glycol)-*b*-poly (butadiene) (PEG-*b*-PBD) with poly (acrylic acid)-*b*-poly (butadiene) (PAA-*b*-PBD), where the two BCPs were homogenously mixed in the polymersome shell.[15] Addition of a cation crosslinks the negatively charged PAA chains, causing strong lateral segregation of the PAA corona domains from that of the PEO. This resulted in porous "patchy" or Janus polymersomes.

Our group has recently developed a miniemulsion crystallization system where a poly (l-lactic acid)-*b*-poly (ethylene oxide) (PLLA-*b*-PEO) was used as a macromolecular surfactant to stabilize the miniemulsion.[18, 19] Carefully controlled crystallization of this system allowed chain folding of the PLLA at the liquid/liquid interface of the emulsion droplets. Crystal growth confined at the curved interface led to the formation of a robust hollow sphere termed "***crystalsome***".[18, 20-22] While these crystalsomes showed interesting mechanical properties,[20, 21] thermal behavior,[23] and excellent performance in blood circulation,[18] the extremely tight packing of the crystalline layer renders the crystalsome shells impermeable to various diffusants, [24, 25] which is undesired from a biomedical application viewpoint. The goal of this work therefore is to introduce porosity to the previously reported single crystal-like crystalsome by employing a secondary BCP in the miniemulsion systems. Our hypothesis is that phase separation between two BCPs at the liquid/liquid interface of an emulsion droplet and subsequently removing the sacrificial BCP could produce a porous structure in the crystalsomes and the competition between crystallization and BCP phase separation could provide an effective means to control the porosity of the crystalline shell. To this end, racemic poly-l,d-lactic acid-*b*-PEO (PLDLA-*b*-PEO) was utilized as the secondary BCP. Miniemulsion consisting of PLLA-*b*-PEO and PLDLA-*b*-PEO was prepared and the emulsion droplets were used as the templates for PLLA crystallization. Porous crystalsomes were obtained after removing uncrystallized PLDLA-*b*-PEO. Crystalsome pore size and pore area fraction were tuned by varying the feed ratio of the two BCPs as well as the crystallization temperature (T_c). We further show that phase separation of two BCPs plays a vital role in controlling the pore formation. Our results demonstrate a new method to prepare porous polymer nanoparticles.

Figure 1a shows a schematic of the crystallization process to form crystalsomes, where a miniemulsion is created by probe sonicating a BCPs/toluene/water mixture. The crystalline amphiphilic BCPs are pinned at the water/oil interface and, upon quenching to T_c, one block of the BCP crystallizes into crystalline lamellae templated by the curved water/oil interface. BCP such as PLLA-*b*-PEO (molar mass of 4.7 kg/mol and 5 kg/mol for PLLA and PEO blocks, respectively) was used as the macromolecular surfactant, BCP crystalsomes were formed with a solid PLLA shell and the PLLA chains are perpendicular to the crystalsome surface.[18] When a second BCP such as PLDLA-*b*-PEO (molar mass of 5 kg/mol for both blocks, PLLA to PLDLA mass ratio *m* is 3:1) is introduced to the system (**Figure 1b**), miniemulsion

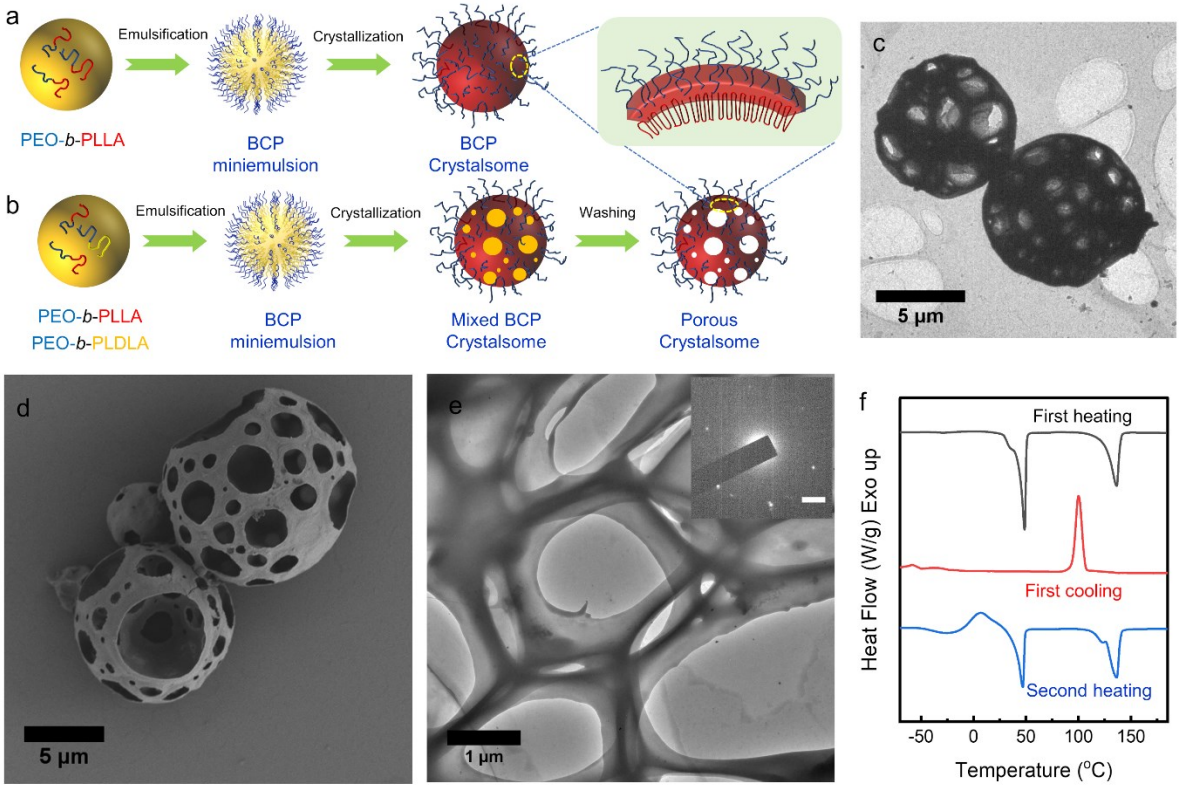

Figure 1. The formation process of BCP porous crystalsomes. (a-b) Schematic process to form (a) crystalsomes with solid shells and (b) porous crystalsomes. (c) TEM and (d) SEM images of PLLA-*b*-PEO porous crystalsomes formed at T_c of 25 °C. (e) Zoomed-in image of a PLLA-*b*-PEO porous crystalsome and the corresponding SAED pattern (inset). (f) DSC thermograms of the PLLA-*b*-PEO porous crystalsomes.

comprised of PLLA-*b*-PEO/PLDLA-*b*-PEO/toluene/water was formed at 94 °C. The racemic PLDLA is miscible with the PLLA block in the miniemulsion system and is excluded from the PLLA lamellae when the emulsion was quenched to 25 °C to crystallize.[19] The sample was then passed through a centrifugal filter tube and thoroughly washed with water to remove the uncrystallized PLDLA-*b*-PEO before being collected for morphology study. The transmission electron microscopy (TEM) image in **Figure 1c** shows spherical, cage-like particles with a diameter of ~ 8-9 μm. The surface of the particles in the image appears dark with high contrast to the background. Scanning electron microscopy (SEM) images in **Figure 1d** better reveals the details of the structure. These particles are apparently hollow and porous with a thin shell. The pore size ranges from sub-microns to ~ 10 microns (Supporting information, **Figure S1**). These pores are evenly distributed on the particle surface. The edges of some pores are smooth while others are rough, likely representing crystal microfacets. The crystalline nature of the particle can be further confirmed using electron diffraction experiments and the results are shown in **Figure 1e**. The zoomed-in TEM image of the particle reveals particle surface with large holes and the corresponding selected area electron diffraction (SAED) pattern in the inset is a typical α phase PLLA [00l] zone pattern.[20, 26] This suggests that the shell of the particle is single crystal-like, consistent with our previous results on homopolymer and BCP crystalsomes.[18, 20] The diffraction spots are relatively sharp, which indicates that no obvious lattice distortion due to the curved shape of the lamellae and this is likely because of the large particle size (hence less lattice distortion).[20, 27] The crystalline nature of the particle can also be confirmed by thermal analysis. **Figure 1f** shows the DSC heating/cooling/heating thermograms of the solution crystallized particles. In the first heating, two endothermic peaks can be seen with melting peaks at 48.7 °C and 136.3 °C, corresponding to the melting of PEO and PLLA crystals, respectively. PEO blocks were crystallized during drying of the samples from emulsion while PLLA crystals were formed during the emulsion solution crystallization. The relative low melting point of PLLA is consistent with our previous BCP crystalsome results, which was attributed to the thinness of the lamella.[18, 22] Atomic force microscopy (AFM) height image in **Figure S2**In the first cooling curve, only PLLA crystallization was observed. The PEO segment showed recrystallization in the second heating thermogram, followed by melting of PEO and PLLA blocks. The above results from morphology, SAED, and DSC confirm the crystalline nature of the porous particles.

Compared with the previously reported crystalsomes with solid shells,[18, 28] the porous particles can be viewed as *porous crystalsomes* (*PCS*). To better discuss the structure, these PCSs are named as *PCS-3L1LD-25*, where *PCS*, *L*, and *LD* denote porous crystalsome, the hydrophobic blocks of the BCP PLLA and PLDLA, respectively. 3 and 1 are from the mass ratio of PLLA to PLDLA in the two BCPs (m = 3:1 in this case), and 25 is T_c. The size distribution of the PCS is

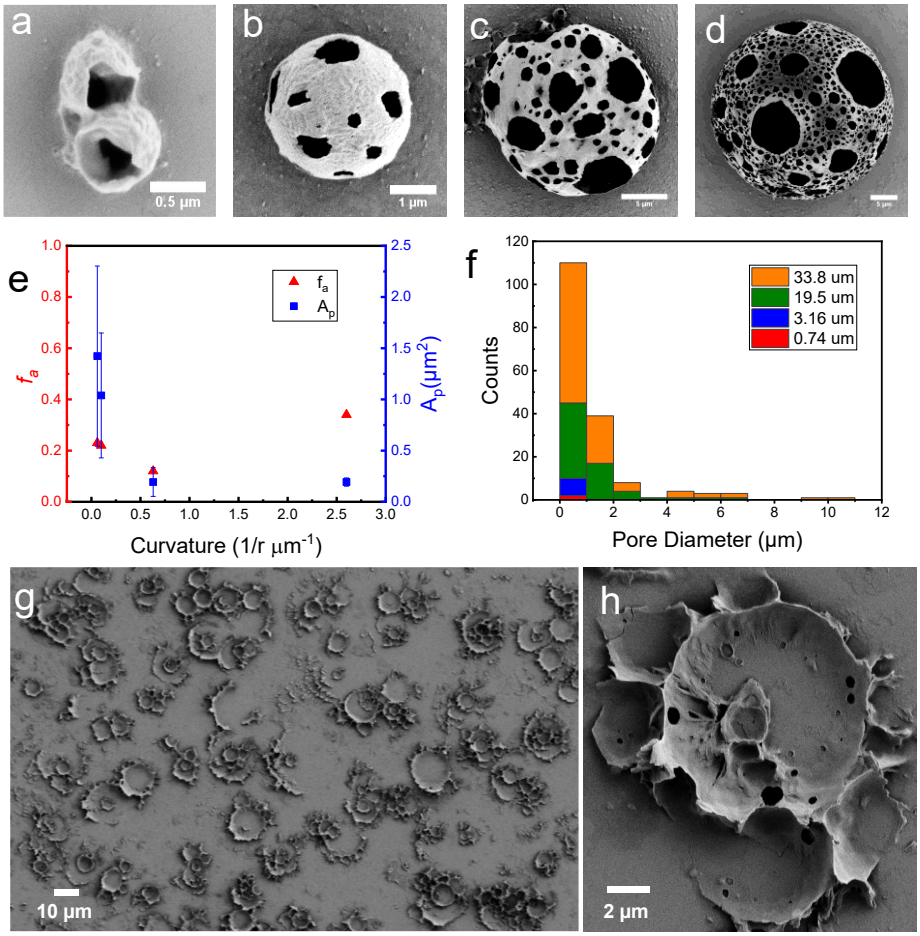

Figure 2. Morphology of the porous crystalsomes. (a-d) Porous crystalsome with different sizes obtained by crystallization at T_c of 25 °C for two days. (e) curvature dependence of the total pore area fraction and pore area of crystalsomes. (f) Histograms of pore size distribution for porous crystalsomes with different diameters. (g-f) Early stages of porous crystalsome by quenching the growth after (g) 20 min, and (h) 2 hrs.

relatively broad --- ranging from a few hundred nanometers to a few microns, as shown in **Figure 2a-d** and **S1**. This is likely due to the broad size distribution of the emulsion droplet templates. The total fraction of the pore area of a PCS (f_a = total pore area/particle surface area) is ~ 0.15-0.3 (**Figure 2e,** see **Figure S3** for detailed calculation), which is similar to the mass fraction of PLDLA in the total hydrophobic components ($\boldsymbol{W_{LD}}$=m_{PLDLA}/m_{PLDLA}+m_{PLLA}) of the two BCPs. Interestingly, the pore area (A_p) is PCS size-dependent: larger pores are observed in large PCSs, and the pore size distribution is nearly bimodal with a few large pores with >4 μm diameter and numerous 1-2 μm pores (**Figure 2f**). This can be attribute to the nucleation and growth mechanism of the phase separation, see later discussion. The formation of the pores on the PCS surface can be attributed to the presence of non-crystalline PLDLA-*b*-PEO, which serves as a "porogen" and is likely to be removed during washing after the crystallization process. PLDLA-*b*-PEO and PLLA-*b*-PEO are uniformly mixed on the surface of an emulsion droplet as PLDLA and PLLA are miscible. Upon crystallization, similar to crystalline polymer blends, PLLA lamellae grow following the water/ toluene interface. This process gradually expels the amorphous PLDLA from the growth front. As the process continues, the excluded PLDLA aggregate on the surface, forming PLDLA-rich domains, which have a rounded disk shape. Removing these domains upon washing leads to the formation of PCSs. To better understand the process, PCSs were collected at early stages of the growth (T_c = 25 °C, crystallization time t =20 min and 2 hrs). Because no external seeds were used during crystallization, we were able to capture a variety of morphologies using a relatively shorter crystallization time. SEM images in **Figures 2g** shows that the bottom of the crystals collapse onto the substrate, forming a flat bottom with uprising rims. The edges of the rims are quite rough, seemly formed by removing rounded PLDLA-*b*-PEO domains that were original expelled to the crystal growth front. In some crystal, the pores began to appear at the rim of the platelet like structures and just inside the rim (**Figure 2h**).

Since PLDLA-*b*-PEO is viewed as the porogen in the PCS formation process and the pores are formed due to PLLA-crystallization-driven BCP phase separation, the mass ratio of the BCPs m and crystallization T_c were tuned to control the morphology of the PCSs. **Figure 3** shows the morphology map of PCSs formed in 12 different conditions. Each row in the figure has a fixed composition (m varied from 1 to 3 to 7 from top to bottom rows) and each column has the same T_c. When m < 1, PCSs were not observed, likely because that the PLLA content was too low to retain the

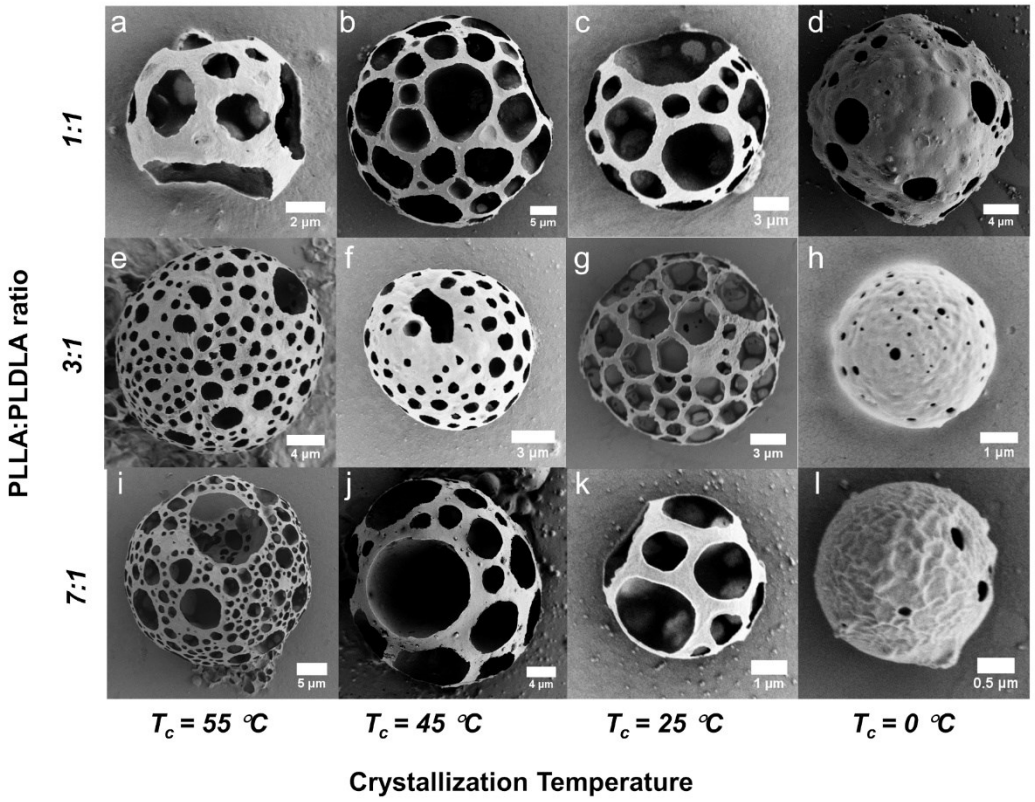

Figure 3. Morphology of porous crystalsomes formed at different PLLA: PLDLA ratio and T_c. (a-d) PLLA: PLDLA = 1:1; (e-h) PLLA:PLDLA = 3:1; (i-l) PLLA:PLALA = 7:1. Tc = 55 °C for (a, e, i), 45 °C for (b, f, j), 25 °C for (c, g, k), and 0 °C for (d, h, l).

spherical morphology of the crystals after removing PLDLA-*b*-PEO during washing (Supporting Information, **Figure S4**). PCSs were observed for m = 1, 3 and 7, as shown in the figure. *PCS-1L1LD-25* and *PCS-7L1LD-25* are similar to the previously observed *PCS-3L1LD-25*, large pores are evident, and the PCSs surfaces are smooth. The pore size and pore surface area A_p are similar although the PLLA to PLDLA ratios were significantly different, suggesting that some of the PLLA-*b*-PEO might have also been removed during the washing process. As we changed T_c from 25 °C to 45 and 55 °C, taking the *PCS-3L1LD* as an example (the middle row in the figure), the PCS morphology remains largely the same. However, when T_c was decreased to 0 °C, a drastically different morphology was seen: only small pores were observed on the crystalsome surface and the total pore areas are also very low. Similar observations were also seen in *PCS-1L1LD and PCS-7L1LD* (top and bottom rows of the figure): the PCS morphology obtained from T_c = 25, 45 and 55 °C is quite consistent with large pores and pore area, while at T_c = 0 °C, the crystalsomes show much smaller pores (**Figure S5** shows DSC heating thermographs of *PCS-3L1LD formed at* T_c = 0, 25, 45 °C. This observation can be explained by consideration of the phase diagram of the two BCPs. **Figure 4** shows a typical phase diagram for a crystalline polymer solution or blend, where both binodal and crystallization lines are shown. The miscibility of the two component polymers affects the relative location of the binodal to the crystallization line. In the system utilized here the good miscibility of the polymers such as a PLLA/PLDLA pair will set the crystallization line above the 2-phase region.[19] Therefore, no phase separation between PLLA and PLDLA is expected in the high temperature region. Upon quenching the miniemulsion system to 0 °C, PLLA will quickly crystallize, and the fast crystallization arrests the PLDLA-*b*-PEO so that limited phase separation between the two BCPs could occur, and the PLDLA-rich domain size therefore is small. Since most of the PLDLA-*b*-PEO is trapped in the PLLA crystals, it's more difficult to remove them during washing, which leads to the final PCSs with limited and small pores. Note that this quenching experiment provides a unique opportunity to fabricate PCSs with small pores. The above discussion suggests that changing PLDLA block to another polymer that is less miscible with PLLA could potentially alter the phase separation/crystallization process and change the PCS morphology. To test this hypothesis, poly(styrene) (PS)-*b*-PEO, with a molar mass of 5k g/mol for each block, was used to replace PLDLA-*b*-PEO in the emulsion. PS and PLLA are immiscible compared to PLDLA and PLLA. **Figure 4b** shows the SEM image of the PCS formed after crystallizing the emulsion at 25°C. The pore size in these PCSs is much smaller compared to the PLDLA case. The other clear feature is the lack of microfacets around the pore edges, which suggests that a phase separation process occurred arresting the PLLA domains followed by the

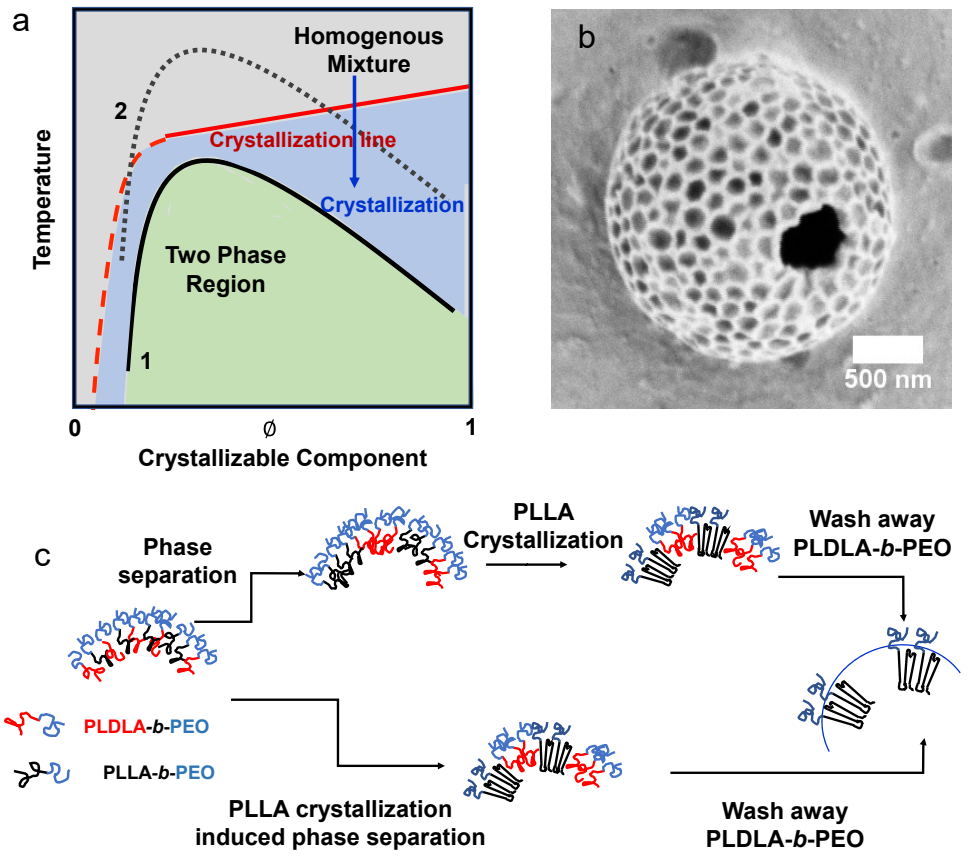

Figure 4. Formation process of porous crystalsomes. (a) schematics of the phase diagram of two BCPs at an emulsion interface. Lines 1 and 2 are binodal lines corresponding to systems with different miscibility. (b) SEM images of a porous crystalsome formed by crystallization of PLLA-*b*-PEO and PS-*b*-PEO emulsions at 25 °C. (c) Two pathways of porous crystals. In the top row, phase separation occurs prior to PLLA crystallization, while the bottom row depicts that PLLA crystallization induced phase separation.

crystallization in those domains. **Figure 4c** summarizes the two different pathways of the PCS formation. We start from high temperature where the two organophilic blocks (either PLLA/PLDLA pair or PLLA/PS pair) are fully dissolved. In the case of PLLA-*b*-PEO/PLDLA-*b*-PEO (pathway 1, bottom), quenching the system to the higher T_c leads to PLLA crystallization, which expels PLDLA from the PLLA crystals. Crystallization-induced phase separation between PLLA and PLDLA then occurs, leading to PLLA-rich and PLDLA rich domains on the surface of the crystalsomes. This process also explains the multimodal nature of the pores because the continuous nucleation and growth of the new PLDLA-rich domains. Therefore, the dispersity and size of the pores in this type of process are dictated by the rate of crystal growth, the nucleation and growth rate of new PLDLA-rich domain, and diffusion of PLDLA molecules at the water/organic interface, which is evident by the morphology variation for PCSs formed at different T_c. In the second pathway where the organophilic blocks are less miscible (PLLA and PS, top row in the figure). In the emulsion formed by of PLLA-*b*-PEO/PS-*b*-PEO. PLLA and PS have a much stronger drive to phase separate, which could quickly take place before PLLA crystallization (pathway 2, top). This leads to PCSs with a small, uniform, and round pore morphology.

In summary, we have shown a new, bottom-up approach to fabricated porous hollow polymer nanoparticles. The structure was formed by controlling the polymer phase separation and crystallization process in a miniemulsion system formed by two amphiphilic BCPs. The competition between BCP phase separation and crystallization led to the formation of unique porous crystalline capsules named as PCSs. The crystalline domain forms the scaffold of the PCSs and the pore sizes can be controlled by tuning BCP phase separation and polymer crystallization. Further work will be conducted to investigate the particle size control and potential applications of these new porous particles.

ASSOCIATED CONTENT

Supporting Information. The Supporting Information is available free of charge on the ACS Publications website at DOI: Experimental details, SEM, AFM and DSC measurement of porous crystalsomes.

AUTHOR INFORMATION

Corresponding Author

* Christopher Y. Li – Email: chrisli@drexel.edu

ACKNOWLEDGMENT

This research was financially supported by the National Science Foundation DMR 2104968 and DMR 1709136.

REFERENCES

1. Wu, D.; Xu, F.; Sun, B.; Fu, R.; He, H.; Matyjaszewski, K., Design and preparation of porous polymers. *Chem. Rev.* **2012,** *112* (7), 3959-4015.
2. Xiang, Z.; Cao, D., Porous covalent–organic materials: synthesis, clean energy application and design. *J. Mater. Chem. A* **2013,** *1* (8), 2691-2718.
3. Silverstein, M. S., PolyHIPEs: Recent advances in emulsion-templated porous polymers. *Prog. Polym. Sci.* **2014,** *39* (1), 199-234.
4. Li, G.; Wang, Z., *Microporous Polyimides with Uniform Pores for Adsorption and Separation of CO2 Gas and Organic Vapors*. 2013; Vol. 46, p 3058–3066.
5. Silverstein, M. S., Emulsion-templated porous polymers: A retrospective perspective. *Polymer* **2014,** *55* (1), 304-320.
6. Dowding, P. J.; Vincent, B., Suspension polymerisation to form polymer beads. *Colloids and Surfaces A: Physicochemical and Engineering Aspects* **2000,** *161* (2), 259-269.
7. Okay, O., Macroporous copolymer networks. *Prog. Polym. Sci.* **2000,** *25* (6), 711-779.
8. Barner, L., Synthesis of Microspheres as Versatile Functional Scaffolds for Materials Science Applications. *Adv. Mater.* **2009,** *21* (24), 2547-2553.
9. Kawaguchi, S.; Ito, K., Dispersion Polymerization. In *Polymer Particles: -/-*, Okubo, M., Ed. Springer Berlin Heidelberg: Berlin, Heidelberg, 2005; pp 299-328.
10. Beneš, M. J.; Horák, D.; Svec, F., Methacrylate-based chromatographic media. *Journal of Separation Science* **2005,** *28* (15), 1855-1875.
11. Vladisavljević, G. T.; Williams, R. A., Recent developments in manufacturing emulsions and particulate products using membranes. *Advances in Colloid and Interface Science* **2005,** *113* (1), 1-20.
12. Oh, J. K.; Drumright, R.; Siegwart, D. J.; Matyjaszewski, K., The development of microgels/nanogels for drug delivery applications. *Progress in Polymer Science* **2008,** *33* (4), 448-477.
13. Shum, H. C.; Abate, A. R.; Lee, D.; Studart, A. R.; Wang, B.; Chen, C.-H.; Thiele, J.; Shah, R. K.; Krummel, A.; Weitz, D. A., Droplet Microfluidics for Fabrication of Non-Spherical Particles. *Macromolecular Rapid Communications* **2010,** *31* (2), 108-118.
14. Seo, M.; Nie, Z.; Xu, S.; Mok, M.; Lewis, P. C.; Graham, R.; Kumacheva, E., Continuous Microfluidic Reactors for Polymer Particles. *Langmuir* **2005,** *21* (25), 11614-11622.
15. Christian, D. A.; Tian, A.; Ellenbroek, W. G.; Levental, I.; Rajagopal, K.; Janmey, P. A.; Liu, A. J.; Baumgart, T.; Discher, D. E., Spotted vesicles, striped micelles and Janus assemblies induced by ligand binding. *Nat. Mater.* **2009,** *8* (10), 843-849.
16. Hsueh, H.-Y.; Yao, C.-T.; Ho, R.-M., Well-ordered nanohybrids and nanoporous materials from gyroid block copolymer templates. *Chem. Soc. Rev.* **2015,** *44* (7), 1974-2018.
17. Hampu, N.; Werber, J. R.; Chan, W. Y.; Feinberg, E. C.; Hillmyer, M. A., Next-generation ultrafiltration membranes enabled by block polymers. *ACS Nano* **2020,** *14* (12), 16446-16471.
18. Qi, H.; Zhou, H.; Tang, Q.; Lee, J. Y.; Fan, Z.; Kim, S.; Staub, M. C.; Zhou, T.; Mei, S.; Han, L., Block copolymer crystalsomes with an ultrathin shell to extend blood circulation time. *Nat. Commun.* **2018,** *9* (1), 3005.
19. Staub, M. C.; Li, C. Y., Confined and Directed Polymer Crystallization at Curved Liquid/Liquid Interface. *Macromol. Chem. Phys.* **2018,** *219* (3), 1700455.
20. Wang, W.; Qi, H.; Zhou, T.; Mei, S.; Han, L.; Higuchi, T.; Jinnai, H.; Li, C. Y., Highly robust crystalsome via directed polymer crystallization at curved liquid/liquid interface. *Nat. Commun.* **2016,** *7*, 10599.
21. Wang, W.; Staub, M. C.; Zhou, T.; Smith, D. M.; Qi, H.; Laird, E. D.; Cheng, S.; Li, C. Y., Polyethylene nano crystalsomes formed at a curved liquid/liquid interface. *Nanoscale* **2018,** *10* (1), 268-276.
22. Qi, H.; Zhou, H.; Tang, Q.; Lee, J. Y.; Fan, Z.; Kim, S.; Staub, M. C.; Zhou, T.; Mei, S.; Han, L.; Pochan, D. J.; Cheng, H.; Hu, W.; Li, C. Y., Block copolymer crystalsomes with an ultrathin shell to extend blood circulation time. *Nature Communications* **2018,** *9* (1), 3005.
23. Staub, M. C.; Li, R.; Fukuto, M.; Li, C. Y., Confined Crystal Melting in Edgeless Poly (l-lactic acid) Crystalsomes. *ACS Macro Lett.* **2020,** *9* (12), 1773-1778.
24. Wang, H.; Keum, J. K.; Hiltner, A.; Baer, E.; Freeman, B.; Rozanski, A.; Galeski, A., Confined crystallization of polyethylene oxide in nanolayer assemblies. *Science* **2009,** *323* (5915), 757-760.
25. Cheng, S.; Li, X.; Zheng, Y.; Smith, D. M.; Li, C. Y., Anisotropic ion transport in 2D polymer single crystal-based solid polymer electrolytes. *Giant* **2020**, 100021.
26. Wang, W.; Qi, H.; Zhou, T.; Mei, S.; Han, L.; Higuchi, T.; Jinnai, H.; Li, C. Y., Highly robust crystalsome via directed polymer crystallization at curved liquid/liquid interface. **2016,** *7*, 10599.
27. Qi, H.; Zhou, T.; Mei, S.; Chen, X.; Li, C. Y., Responsive Shape Change of Sub-5 nm Thin, Janus Polymer Nanoplates. *ACS Macro Lett.* **2016,** *5* (6), 651-655.
28. Qi, H.; Liu, X.; Henn, D. M.; Mei, S.; Staub, M. C.; Zhao, B.; Li, C. Y., Breaking translational symmetry via polymer chain overcrowding in molecular bottlebrush crystallization. *Nat. Commun.* **2020,** *11* (1), 2152.

SYNOPSIS TOC